Redox-mediated electrosynthesis of ethylene oxide from CO$_2$ and water

Yuhang Li [1,2,7], Adnan Ozden[3,7], Wan Ru Leow [1,4,7], Pengfei Ou [1,7], Jianan Erick Huang[1], Yuhang Wang[1], Koen Bertens[1], Yi Xu [3], Yuan Liu [1], Claudie Roy[5], Hao Jiang [2,6], David Sinton [3], Chunzhong Li [2,6] ✉ and Edward H. Sargent [1] ✉

The electrochemical production of ethylene oxide (EO) from CO$_2$, water and renewable electricity could result in a net consumption of CO$_2$. Unfortunately existing electrochemical CO$_2$-to-EO conversions show impractical Faradaic efficiency (FE) and require a high energy input. Here we report a class of period-6-metal-oxide-modified iridium oxide catalysts that enable us to achieve improved CO$_2$-to-EO conversion. Among barium, lanthanum, cerium and bismuth, we find that barium-oxide-loaded catalysts achieve an ethylene-to-EO FE of 90%. When we pair this with the oxygen reduction reaction at the cathode, we achieve an energy input of 5.3 MJ per kg of EO, comparable to that of existing (emissions-intensive) industrial processes. We have also devised a redox-mediated paired system that shows a 1.5-fold higher CO$_2$-to-EO FE (35%) and uses a 1.2 V lower operating voltage than literature benchmark electrochemical systems.

The manufacture of chemicals produces a significant global carbon footprint:[1–3] for example, direct CO$_2$ emissions from the production of high-value chemicals (that is, ethylene, propylene and benzene/toluene/xylene derivatives) now exceed 200 Mt yr^{-1}. In the case of ethylene oxide (EO), a commodity chemical produced at the rate of 20 Mt yr^{-1} for the manufacture of polyethylene terephthalate, the steam cracking process emits ~1–2 tCO$_2$ per tonne of ethylene (C$_2$H$_4$) produced, and the direct C$_2$H$_4$ oxidation process emits ~0.9 tCO$_2$ per tonne of EO produced[4].

Renewable-electricity-powered electrochemical processes convert waste CO$_2$ emissions into valuable chemicals and fuels such as C$_2$H$_4$, ethanol and acetate[5], enabling a reduction in net CO$_2$ emissions. Additional CO$_2$ savings can be achieved by electrifying the upgrade of chemicals to higher-value commodities such as EO[6–10]. For instance, the synthesis of EO from CO$_2$, water and renewable electricity can consume of 2 tCO$_2$ tEO^{-1}, in contrast to the emission of ~2 tCO$_2$ tEO^{-1} from the existing process.

The electrosynthesis of EO from CO$_2$ is currently achieved using two independent electrolysers: in the first CO$_2$ is reduced to C$_2$H$_4$; in the second C$_2$H$_4$ is oxidized to EO (ethylene oxidation reaction (EtOR))[6]. While the EtOR (Fig. 1a) was achieved at a high (1 A cm^{-2}) current density, the total CO$_2$-to-EO Faradaic efficiency (FE) was limited to 6% when operated at a high CO$_2$ gas flow rate of 50 sccm (calculated from the FE for CO$_2$-to-C$_2$H$_4$ reduction multiplied by the FE for C$_2$H$_4$-to-EO oxidation)[6]. This literature benchmark system suffers from a major missing FE component in C$_2$H$_4$-to-EO, the loss here exceeding 80%, the result of hypochlorous acid (HOCl) cleavage to unreactive ClO$^-$ in the EtOR. As a result, the energy required is ~19 MJ per kg of EO, approximately five times more

energy-intensive than the existing thermochemical route at ~4 MJ per kg of EO (ref. [7]).

In this article we prepare catalysts by loading a class of period-6-metal oxides on IrO$_2$. We find that barium-oxide-loaded catalysts suppress HOCl cleavage and improve the C$_2$H$_4$-to-EO FE. Moving the cathode reaction over to oxygen reduction enables a total CO$_2$-to-EO FE of 35% with a 1.2 V lower operating voltage compared with previous literature[6].

Results

Tuning HOCl cleavage energy on period-6-metal oxides. We first studied the HOCl cleavage process on bare IrO$_2$ with the aid of density-functional theory (DFT) calculations: both perfect and oxygen-vacancy-bearing IrO$_2$ surfaces presented a spontaneous reaction for *HOCl → *H + *OCl with negative values in Gibbs free energy change (ΔG) (Fig. 1b and Supplementary Fig. 1). The negative ΔG explains the low FE of EO on bare IrO$_2$ catalyst reported previously[6], which arises from HOCl-to-ClO$^-$ cleavage (Fig. 1c).

We therefore looked for ways to enhance the FE of EO on IrO$_2$ catalysts. By loading four period-6-metal oxides (barium, lanthanum, cerium and bismuth oxides)—known to possess good stability in chlorine solution—as promoter candidates, we sought to influence the thermodynamics of HOCl cleavage and to maintain the HOCl generation capacity. We studied these four period-6-metal-oxide-loaded catalysts (Supplementary Figs. 2–4) and investigated their performance in the electrochemical production of EO from C$_2$H$_4$ (Supplementary Fig. 5).

Of these catalysts, the barium-oxide-loaded IrO$_2$ (BaO$_x$/IrO$_2$) showed the best results: it limited the FE toward unreactive ClO$^-$ to below 10%, thus increasing the C$_2$H$_4$-to-EO FE to 90% (Fig. 1d).
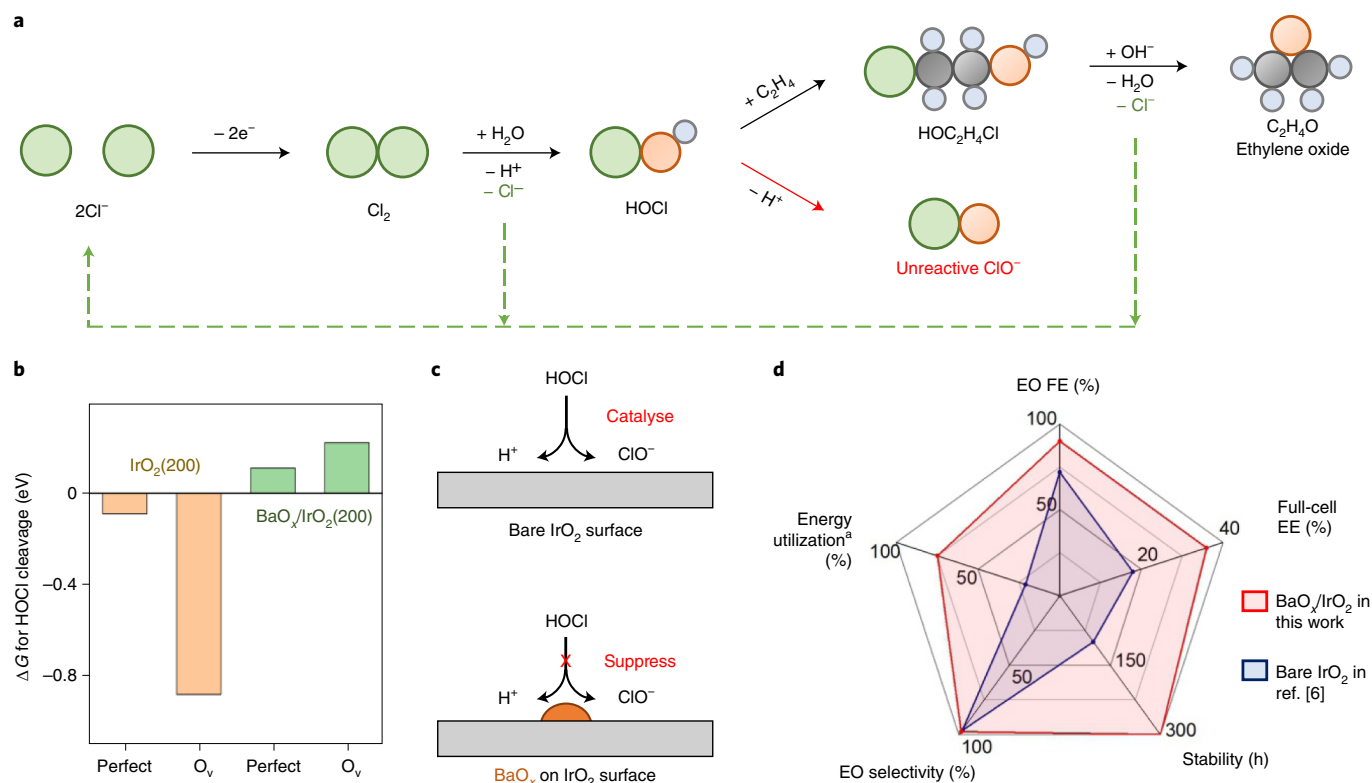
Fig. 1 | Comparison of BaO$_x$/IrO$_2$ and bare IrO$_2$ electrocatalysts. a, Key reaction pathway to produce EO using HOCl as the key intermediate. The HOCl-to-ClO$^-$ cleavage will result in loss of FE toward the desired product EO. Green, chlorine; orange, oxygen; light blue, hydrogen; grey, carbon. **b**, Gibbs free energy changes (ΔG) of the reaction *HOCl → *H + *OCl on bare IrO$_2$(200) and Ba$_3$O$_4$-cluster-loaded IrO$_2$(200) with perfect and oxygen-vacancy (O$_v$) surfaces. **c**, Schematic HOCl cleavage process on bare IrO$_2$ and BaO$_x$/IrO$_2$ surfaces. Undesired HOCl cleavage can be suppressed using BaO$_x$/IrO$_2$ and is facilitated by bare IrO$_2$. **d**, EO FE, full-cell EE, stability, EO selectivity and energy utilization compared to best prior results for EO electrosynthesis. Data are collected at the same applied current density of 100 mA cm^{-2}. ^{a}Normalization: for energy utilization, 100% represents the direct C$_2$H$_4$ oxidation process (the corresponding energy consumption is ~4 MJ per kg of EO produced).

DFT results show positive ΔG for HOCl cleavage on both perfect and oxygen-vacancy-bearing BaO$_x$/IrO$_2$ interfaces, suggesting that this undesired reaction becomes no longer spontaneous (Fig. 1c), thus enhancing the FE of EO (Supplementary Note 1).

We then characterized BaO$_x$/IrO$_2$ catalysts and determined a Ba/Ir ratio of ~3 wt% (see Methods for details). The X-ray diffraction pattern suggests the presence of amorphous BaO$_x$ species ($x = 1$–2) in the catalyst (Supplementary Fig. 6). We further explored the structure and composition of the catalyst by transmission electron microscopy (TEM) (Fig. 2a–d): the Ir, Ba and O are homogeneously dispersed throughout the nanoparticle-like catalyst, and a BaO$_x$ nanoparticle ~30 nm in size is found in Fig. 2c. This suggests that some of the BaO$_x$ nanoparticles are loaded onto IrO$_2$, rather than Ba doping the IrO$_2$ lattice. This can be accounted for by reference to the large difference in the atomic radii (268 pm for Ba and 202 pm for Ir). We measured the lattice fringes to be 0.23 nm (Fig. 2e), and associate these with IrO$_2${200} facets[11]. We then investigated the valence state of each element in the BaO$_x$/IrO$_2$ catalyst by X-ray photoelectron spectroscopy (XPS), which indicated that Ir and Ba were in the IV and II oxidation states, respectively (Fig. 2f,g)[12,13]. In addition, the O 1s XPS peak is assigned to the OH–Ir and O–Ir bonds (Fig. 2h)[12]. Based on these findings, we concluded that the catalyst is composed of BaO$_x$ ($x = 1$–2) nanoparticles loaded onto IrO$_2$.

Performance in EO electrosynthesis. We evaluated the performance of BaO$_x$/IrO$_2$ in a two-electrode flow-cell set-up (see Methods for details) using a titanium mesh substrate (Supplementary Fig. 7). As presented in Fig. 3a, at current densities ranging from 100 to

1,500 mA cm^{-2}, the FEs of C$_2$H$_4$-to-EO conversion on BaO$_x$/IrO$_2$ catalyst are >85% and reach a plateau of 90% $\pm$ 1% at 200 mA cm^{-2}. On the IrO$_2$/Ti control, the FEs for EO are ~65% in the same current density range, consistent with the performance reported in recent work[6]. We limited the FE toward unreactive ClO$^-$ to below 10% on BaO$_x$/IrO$_2$ electrocatalyst, thus reducing the aqueous waste streams by more than three-fold compared with the bare IrO$_2$ catalyst, which had an FE of ~30% for ClO$^-$. We also found, by conducting in situ Raman measurements (Supplementary Fig. 8), that the Ba–O–Cl structure[14] is formed on BaO$_x$/IrO$_2$ catalysts during reaction, consistent with the models suggested by DFT calculations (Supplementary Fig. 1).

We noted that the product selectivity in the C$_2$H$_4$-to-EO conversion is 98% $\pm$ 0.3%, with no overoxidation to CO$_2$ detected. We also investigated the performance of BaO$_x$/IrO$_2$ catalysts with different BaO$_x$ loadings (from 1 to 4 wt%) in various anolyte concentrations (from 1 to 3 M KCl) (Supplementary Fig. 9). Of the catalysts, 3 wt% BaO$_x$/IrO$_2$ in 2 M KCl anolyte exhibits the highest performance. This enables an EO full-cell energy efficiency (EE) of 36% (non-iR-corrected; i, current (in amps); R, resistance (in ohms)) at 100 mA cm^{-2} (Fig. 3b), representing a 2.5-fold improvement in EE compared with literature benchmark systems operating under similar reaction rates (Supplementary Table 1)[6].

We carried out a technoeconomic assessment (Supplementary Note 2) to assess the contribution of the BaO$_x$/IrO$_2$-promoted performance to total plant-gate levelized cost (PGLC, Fig. 3b)[15]. Using an electricity price of US$0.05 kWh^{-1} (refs. [6,15]), we found that the system equipped with the BaO$_x$/IrO$_2$ catalyst is projected—for a wide current density range of 100 to 1,500 mA cm^{-2}—to enable a
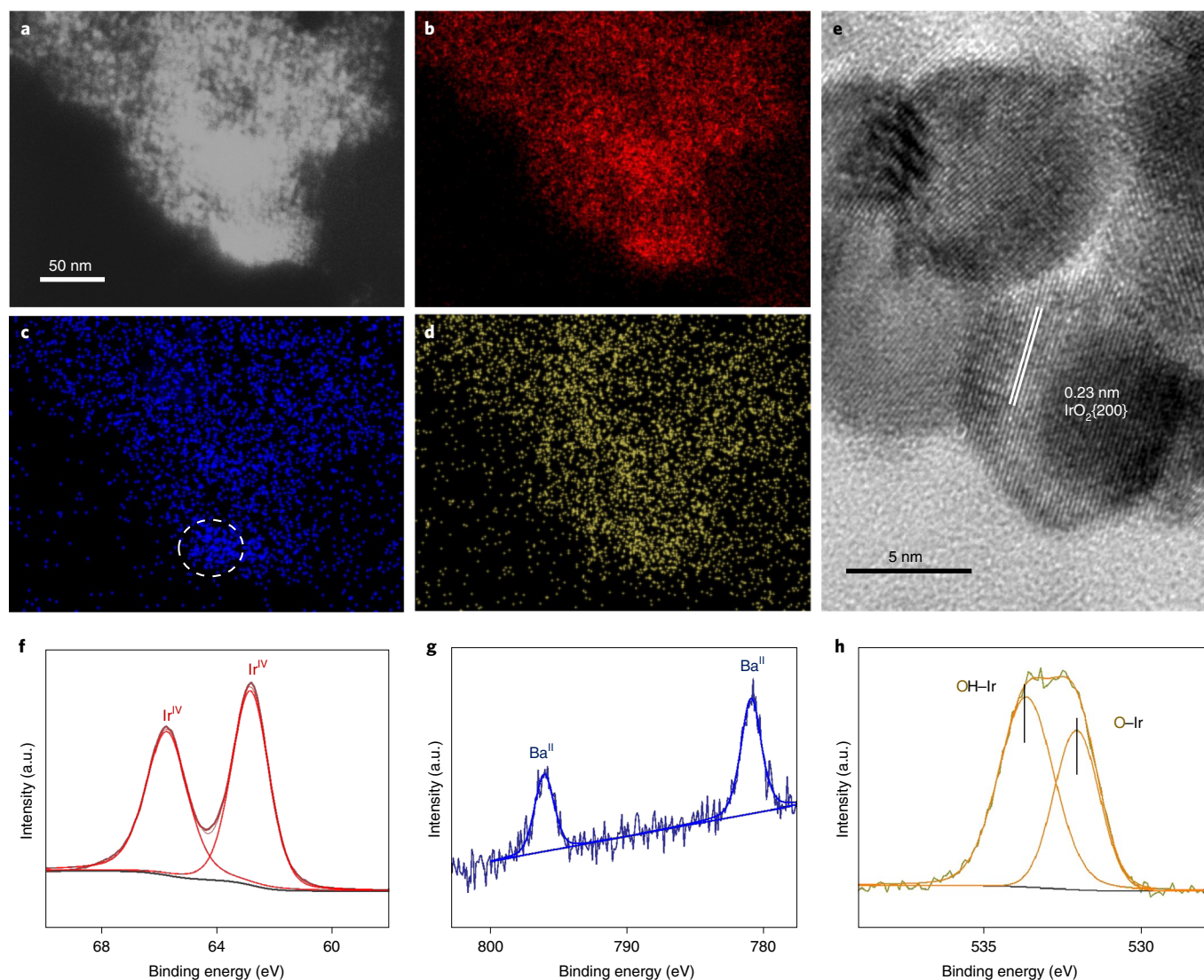
Fig. 2 | Characterization of BaO$_x$/IrO$_2$ electrocatalysts. a–d, Electron microscopy of BaO$_x$/IrO$_2$ catalysts: STEM image (**a**) and elemental mapping of Ir (**b**), Ba (**c**) and O (**d**). The dotted circle in **c** indicates BaO$_x$ nanoparticles. **e**, High-resolution TEM of BaO$_x$/IrO$_2$ catalyst. **f–h**, Ir 4f (**f**), Ba 3d (**g**) and O 1s (**h**) XPS spectra of the as-prepared BaO$_x$/IrO$_2$ catalyst.

production cost that is lower than the combined market value of EO per tonne and corresponding cathodic H$_2$ produced (US$1,486).

We then turned our focus to assessing the stability of the system. We performed the extended operation at a current density of 100 mA cm^{-2}, where the system delivers the highest full-cell EE with profitable PGLC. The catalyst maintains an average FE of EO of >85% and a selectivity of ~98% for 300 h of continuous operation with a full-cell voltage of ~3.2 V (non-*iR*-corrected) (Fig. 3c). We then analysed the structure and composition of the BaO$_x$/IrO$_2$ catalyst upon completion of the extended operation. The X-ray diffraction pattern, the XPS spectra and TEM images of the catalyst (Supplementary Fig. 10) suggest no obvious changes in elemental valence state, element distribution and nanoparticle-like structure. Post-reaction inductively coupled plasma atomic emission spectroscopy analysis of the catalysts indicates that the catalyst preserves its original barium loading of ~3 wt% for 300 h of uninterrupted electrooxidation.

We detected ethylene chlorohydrin (HOC$_2$H$_4$Cl)—formed from the reaction between HOCl and C$_2$H$_4$ (Supplementary equation (3) in Supplementary note 1)[16]—as the only anodic product during electrolysis (Supplementary Fig. 11). We thus concluded that the

final FE of EO is only related to the amount of HOCl, because the Cl$_2$ will convert C$_2$H$_4$ to ethylene dichloride, which is not detected, while the other species in the anolyte (such as Cl$^-$ and ClO$^-$ anions) are unreactive to C$_2$H$_4$.

We also provided the EO production performance in acidic electrolytes (pH 3 and 5; Supplementary Table 2); we found that no EO is produced. We attribute this to the absence of OH$^-$ in acidic catholytes (Supplementary equation (4) in Supplementary note 1) and hence the suppressed conversion of HOC$_2$H$_4$Cl into EO (Supplementary equation (5) in Supplementary note 1).

Full-cell optimization via anodic EtOR with the cathodic oxygen reduction reaction. Although we increased the C$_2$H$_4$-to-EO FE to 90% by using BaO$_x$/IrO$_2$ catalyst, the energy input (~9 MJ per kg of EO) is still 2.2-fold higher than that of the current thermochemical processes. We noted that the anodic EtOR coupled with the hydrogen evolution reaction (HER) requires a high theoretical reaction potential of 1.36 V (Fig. 4a), undesirably increasing the full-process energy requirement by producing the by-product H$_2$. We posited that if we could—without sacrificing the FEs and production rates of EO—displace the HER at the cathode with a
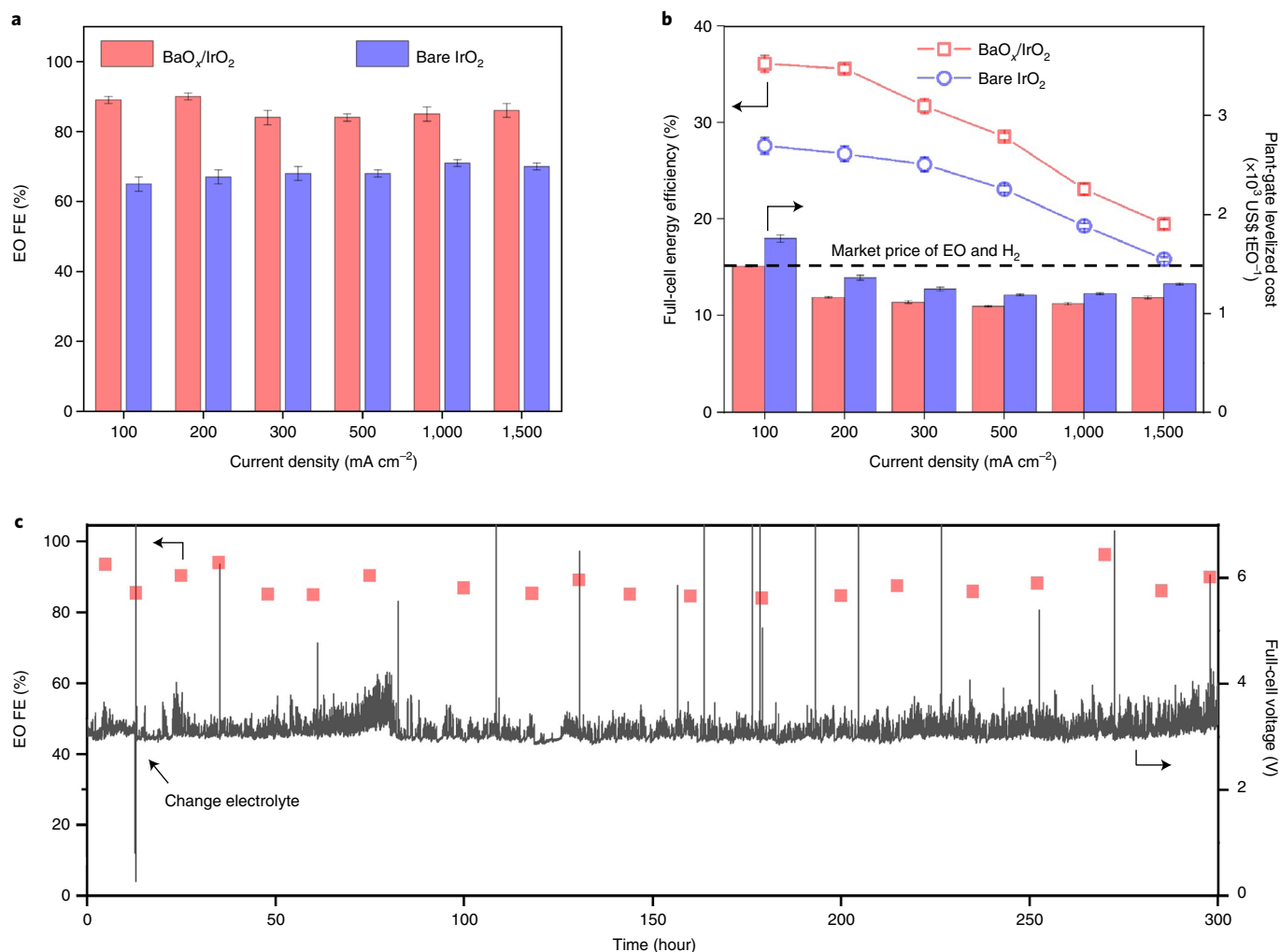
Fig. 3 | Electrochemical performance of BaO$_x$/IrO$_2$ electrocatalysts. a,b, The FE of EO (**a**) and the full-cell energy efficiency and PGLC (**b**) using BaO$_x$/IrO$_2$ catalysts compared with bare IrO$_2$ sample at different applied current densities in 2 M KCl electrolyte. The electricity cost was set at US$0.05 kWh^{-1}. **c**, Stability test for EO during 300 h of electrolysis under a current density of 100 mA cm^{-2} in 2 M KCl electrolyte. All voltages are non-*iR*-corrected. Error bars represent the s.d. from three independent measurements. Pink squares in **c** represent the EO FE. Right-angled arrows in **b** and **c** indicate the axis that is being referred to.

lower-thermodynamic-potential reaction, we would significantly reduce the energy input of the C$_2$H$_4$-to-EO conversion.

We thus replaced the HER with the oxygen reduction reaction (ORR), enabling a theoretical reaction potential of 0.13 V (Fig. 4a). At applied current densities of 100, 200 and 300 mA cm^{-2}, the FEs of the C$_2$H$_4$-to-EO conversion were >80% with full-cell voltages of 2.0, 2.2 and 2.4 V, respectively (Fig. 4b).

The full-cell voltage is reduced by 1.2 V compared with that of the best previous report that relied on cathodic HER (Supplementary Fig. 12)[6]. The reduction in the operating voltage in turn leads to an energy saving of 5.4 kMJ per tonne of EO produced—an energy saving that corresponds to the energy required to produce H$_2$ in the cathodic HER case (0.045 tH$_2$tEO^{-1}, equivalent to an energy of 5.4 kMJ tEO^{-1}). The reduced voltage results in a PGLC reduction of US$110 tEO^{-1}, and the loss in economic value by stopping H$_2$ production (0.045 tH$_2$tEO^{-1}, with a value of US$90 tEO^{-1}) is less than the saving in cost resulting from the lower reaction potential (Supplementary Fig. 13).

With the benefit of cathodic ORR, PGLCs in the current density range 100–300 mA cm^2 are projected to be profitable, with a low electrical energy input of 5.3 MJ kgEO^{-1} (Fig. 4c), representing a 3.6-fold reduction in the energy intensity compared with the benchmark electrochemical process[6]. This energy intensity is close to that of the conventional emissions-intensive industrial process for producing

EO (~4 MJ kgEO^{-1})[7]. It should be noted that in this electrochemical system we used the same gas feeds as the industrial direct oxidation process (air and ethylene) for producing EO with an EO selectivity of 98% while that in industry is <80%. The system was stable, maintaining an average FE of EO of >80% and a full-cell voltage of ~2 V at an applied current density of 100 mA cm^{-2} for over 100 h (Fig. 4d).
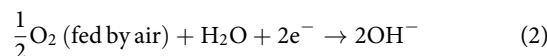
Oxygen-redox-mediated paired system for CO$_2$-to-EO conversion. To test the configuration of an cathodic ORR and an anodic EtOR, we built an oxygen redox (H$_2$O/O$_2$)-mediated paired system to produce EO from CO$_2$ (Fig. 4e and Supplementary Fig. 14). The CO$_2$-to-C$_2$H$_4$ reduction in chamber 1 with C$_2$H$_4$-to-EO oxidation in chamber 2 are connected by the H$_2$O/O$_2$ mediator that cycles between the oxygen evolution reaction (OER) and the ORR (equations (1)–(3)).

On the anode side of chamber 1 for producing 1 mol of C$_2$H$_4$:

$$6H_2O \rightarrow 3O_2 + 12H^+ + 12e^- \tag{1}$$
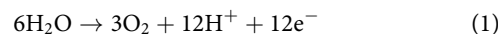
On the cathode side of chamber 2 for producing 1 mol of EO:

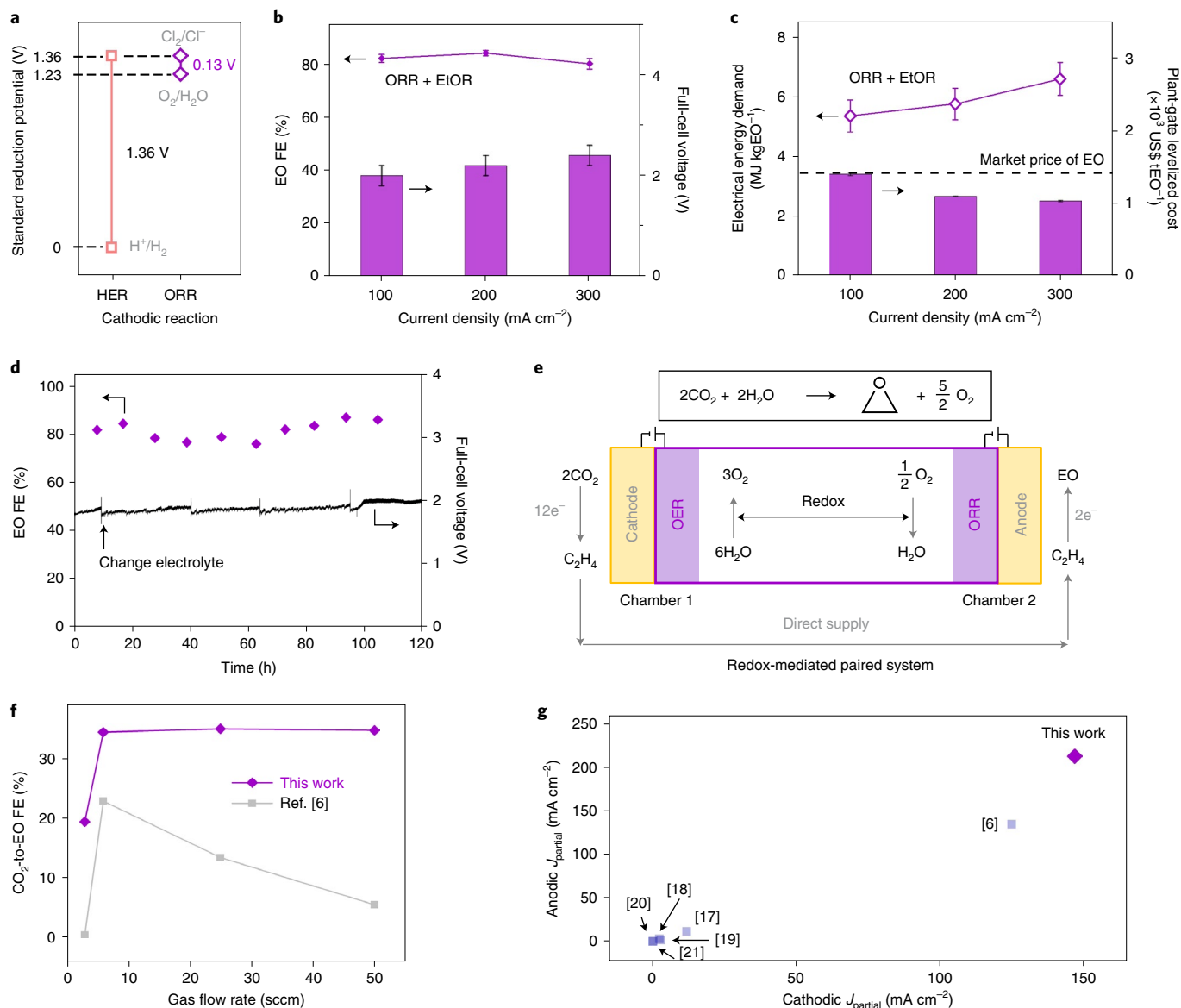$$\frac{1}{2}O_2 \text{ (fed by air)} + H_2O + 2e^- \rightarrow 2OH^- \tag{2}$$

Fig. 4 | Coupling with cathodic ORR and redox-mediated paired system. a, Theoretical reaction potentials for producing EO for cathodic HER or ORR. **b,c**, The FE of EO and corresponding full-cell voltage (**b**) and electrical energy demand and PGLC (**c**) when coupled with the cathodic ORR at different applied current densities in 2 M KCl electrolyte. The electricity cost was set at US\$0.05 kWh⁻¹. **d**, Stability test for the production of EO during 100 h of electrolysis with cathodic ORR under a current density of 100 mA cm⁻² in 2 M KCl electrolyte. **e**, Total reaction equation and schematic description of the electrochemical process to produce EO from CO_2 using a redox-mediated paired system with an oxygen redox mediator. **f**, Comparison of CO_2-to-EO FEs using the BaO_x/IrO_2 catalysts described in this paper relative to that in the highest-performing previous reports of EO production from CO_2 and water[6]. The downstream of the CO_2RR electrolyser was sparged into the anolyte of the C_2H_4-to-EO oxidation flow cell (current density, 300 mA cm⁻²) for all CO_2 flow rates studied and was used without purification. **g**, Reported cathodic and anodic partial current densities for other paired systems combining the CO_2RR with anodic upgrading reactions[6,17–21] (square brackets are reference numbers). Data for the redox-mediated paired system are shown in **g** for comparison (purple). All voltages are non-*iR*-corrected. Error bars represent the s.d. from three independent measurements. Arrows in **b** and **c**, and right-angled arrows in **d** indicate the axis that is being referred to.

In the H_2O/O_2 mediator (combining equations (1) and (2)):

$$5H_2O \rightarrow \frac{5}{2}O_2 + 10H^+ + 10e^- \qquad (3)$$
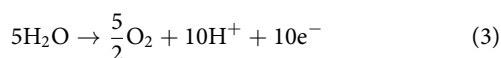
Two approaches have been developed to produce EO from CO_2 by electrochemical means (Table 1, Supplementary Fig. 15 and Supplementary Note 3). The first involves two independent electrolysers: one for the CO_2 reduction reaction (CO_2RR) coupled with the OER, and another for the EtOR coupled with the HER.

The second approach involves directly coupling the CO_2RR and the EtOR in one electrolyser. However, the first approach requires an added theoretical reaction potential of 1.23 V (Fig. 4a), and the second approach has a current matching issue that limits the anodic FE of EO to a maximum of ~17% (Supplementary note 4 and Supplementary Table 3).

The oxygen-redox-mediated paired system overcomes the above problems: we maintained a low theoretical reaction potential of 1.28 V for CO_2-to-C_2H_4 reduction with C_2H_4-to-EO oxidation (Table 1), and overcame the larger electron consumption in CO_2-to-C_2H_4

Table 1 | Electrochemical systems to produce EO from CO_2

	Redox-mediated paired system	Two independent electrolysers	One electrolyser
Cathode 1	CO_2-to-C_2H_4	CO_2-to-C_2H_4	CO_2-to-C_2H_4
Anode 1	OER	OER	Cl_2 evolution reaction (for C_2H_4-to-EO)
E_1° (V)	1.15	1.15	1.28
Cathode 2	ORR	HER	–
Anode 2	Cl_2 evolution reaction (for C_2H_4-to-EO)	Cl_2 evolution reaction (for C_2H_4-to-EO)	–
E_2° (V)	0.13	1.36	–
E_T° (V)[a]	1.28	2.51	1.28
Advantages/ challenges	• Low theoretical reaction potential to produce EO from CO_2 • All chambers are able to run in optimal conditions without cross-interference	• All cells are able to run in optimal conditions without cross-interference • High PGLC for producing EO	• Low theoretical reaction potential to produce EO from CO_2 • FE upper limit of ~17% • Cross-interference (carbonate formation)

[a]$E_T^\circ = E_1^\circ + E_2^\circ$. E_1°, E_2° and E_T° are the theoretical reaction potentials for chamber 1, chamber 2 and total system, respectively. At pH 7, the E° (standard reduction potential) of H^+/H_2, O_2/H_2O, Cl_2/Cl^- and CO_2/C_2H_4 is −0.42, 0.81, 0.94 and −0.34 V, respectively.

($12e^-$) versus C_2H_4-to-EO ($2e^-$) by converting more H_2O into O_2, rendering H_2O as the only sacrificial agent (equation (3)).

The redox-mediated electrochemical system also enables the synthesis of EO from CO_2, water and renewable electricity with a consumption of $2 \, tCO_2 \, tEO^{-1}$, in contrast to total emissions of 2.0–$2.7 \, tCO_2 \, tEO^{-1}$ and direct emissions of $0.55 \, tCO_2 \, tEO^{-1}$ in the existing thermochemical processes (Supplementary Fig. 16 and Supplementary Tables 4 and 5).

We produced C_2H_4 with ~45% FE from the CO_2RR at different current densities and found that the cathode and anode in chamber 1 maintain stable operation for 100 h of the CO_2RR (Supplementary Figs. 17–19 and Supplementary Table 6). We achieved a total CO_2-to-EO FE of ~35% by using the electrocatalytically generated C_2H_4 from chamber 1 at a current density of $300 \, mA \, cm^{-2}$ with different CO_2 gas flow rates (Fig. 4f, Supplementary Fig. 20 and Supplementary Table 7). We note, for comparison, that this EO productivity is >1.5-fold higher than that reported in the literature benchmark electrocatalytic CO_2-to-EO conversion system[6].

We also compared the performance of the redox-mediated paired system with previously described paired systems combining the CO_2RR with anodic upgrading reactions[6,17–21]. With a total current density of $300 \, mA \, cm^{-2}$ and high FEs, we achieved partial current densities of 147 and $213 \, mA \, cm^{-2}$ for the cathodic C_2H_4 product and anodic EO product, respectively. These outperform by 1.5-fold the best previous reports of paired systems that combine CO_2 reduction with anodic upgrading (Fig. 4g and Supplementary Tables 8 and 9).

Discussion

In this work we sought to address the limitations of electrochemical production of EO from CO_2: we achieved an FE for CO_2-to-EO conversion that enables a 1.5-fold higher productivity compared with literature benchmark electrochemical systems. We presented a surface-modification strategy to enhance the electrosynthesis of EO

on period-6-metal-oxide-loaded IrO_2. Using this strategy, we found that the BaO_x/IrO_2 interface serves to block the HOCl cleavage pathway. The catalysts achieved an FE for EO of 85–91%, higher than that for the bare IrO_2 studied in our previous work[6], and a selectivity of 98% in the current density range of 100–$1,500 \, mA \, cm^{-2}$. We obtained a stable full-cell EE of 36% at $100 \, mA \, cm^{-2}$ for 300 h with the cathodic HER. By switching the cathodic reaction to the ORR, we achieved a 1.2 V reduction in the full-cell voltage, enabling a low energy input of 5.3 MJ per kg of EO produced electrochemically, representing a 3.6-fold reduction in energy intensity compared with the benchmark electrochemical process[6]. We further devised an O_2-redox-mediated paired system comprising CO_2-to-C_2H_4 reduction and C_2H_4-to-EO oxidation with a total FE of ~35% for complete CO_2-to-EO conversion, which means that high-rate, efficient and stable electrosynthesis of EO can be achieved by using CO_2, H_2O and renewable electricity as the only consumables.

Methods

Materials preparation. The electrodes for the anodic reaction were prepared by a five-step procedure. We begin by etching the titanium mesh in 3 M HCl (≥98%, Sigma Aldrich) at 75 °C for 40 min. We then soak this etched mesh in a well-mixed solution of iridium(IV) oxide dehydrate (99.99%, Alfa Aesar), HCl (ACS reagent, 37%) and barium chloride dihydrate (>99.999%) (with various wt% ratios) in isopropanol (Sigma Aldrich). We then dry the resulting titanium mesh at 120 °C and sinter it at 500 °C to obtain BaO_x/IrO_2 catalyst on titanium mesh (IrO_2/Ti). Finally, we repeat the soaking, drying and sintering steps until the target BaO_x/IrO_2 loading of $2 \, mg \, cm^{-2}$ is achieved. IrO_2/Ti electrodes were prepared by following a procedure similar to that described above, except that we instead incorporated barium chloride dihydrate salt into the catalyst ink. For X-ray diffraction measurements, a similar procedure was followed but with the BaO_x/IrO_2 catalyst supported on a hydrophilic carbon cloth (CT Carbon Cloth without MPL, Fuel Cell Store) instead of a titanium mesh, and then extracted from the surface of the carbon cloth upon completion of the synthesis. For other metal-oxide-loaded catalysts, we changed the barium precursor to 3 wt% of the corresponding metal chloride (such as lanthanum(III) chloride hydrate (99.9%), cerium(III) chloride (99.9%) and bismuth(III) chloride (99.99%)).

Electrode preparation for the redox-mediated paired system. The electrodes for the CO_2RR (chamber 1, cathode) were prepared by a two-step procedure. In the first step, copper/polytetrafluoroethylene (PTFE) electrodes were prepared by evaporating a copper target (Kurt J. Lesker) onto a hydrophobic PTFE substrate (average pore size, 450 μm) with a constant sputtering rate of $0.5 \, \text{Å} \, s^{-1}$ at 10^{-6} torr until the desired thickness of 150 nm was achieved. In the second step, copper nanoparticle/copper/PTFE electrodes were prepared by spray-depositing a homogeneous solution of copper nanoparticles (Sigma Aldrich, 25 nm) and a polymeric binder (Aquivion D79-25BS, Sigma Aldrich) onto the copper/PTFE substrate until a catalyst loading of $1.25 \, mg \, cm^{-2}$ was achieved.

The electrodes for the OER (chamber 1, anode) are similar to the above IrO_2/Ti electrodes. To make the electrodes for the HER and ORR (chambers 1 and 2, cathode), a well-mixed solution of commercially available platinum supported on graphitized carbon (40% Pt on Vulcan XC72, Sigma Aldrich) and polymeric binder (Aquivion D79-25BS, Sigma Aldrich) was spray-deposited on a superhydrophobic gas diffusion layer on a heated vacuum plate at 50 °C. The deposition was continued until a platinum loading of $0.4 \, mg \, cm^{-2}$ was achieved.

Materials characterization. TEM imaging and energy-dispersive X-ray analysis elemental mapping were carried out using a field emission transmission electron microscope (Hitachi HF3300). SEM images were obtained with a Hitachi S-5200. X-ray diffraction was performed on a MiniFlex600 spectrometer with Cu Kα radiation. XPS was conducted on a Thermo Scientific K-Alpha XPS system using Al Kα X-ray radiation (1,486.6 eV) for excitation. The loading was detected via inductively coupled plasma atomic emission spectroscopy. In situ Raman spectroscopy was performed using a Renishaw inVia Raman microscope with a water immersion objective (785 nm laser) in a home-made flow cell (Supplementary Fig. 8b).

Electrochemical tests. Ethylene oxidation experiments were carried out in a flow cell equipped with an anode electrode (IrO_2/Ti), an anion-exchange membrane (Fumasep FAB-PK-130) and a cathode electrode (40% Pt on Vulcan XC72). We fabricated the cathodic and anodic flow-field plates for electrolyte delivery with thicknesses of 1.5 and 5 mm, respectively. With the thicker anodic plate, we aimed to prevent membrane leaching potentially caused by the chlorine generated in the electrochemical reaction (Supplementary equation (1) in Supplementary note 1). We fed the cathode electrode with air for the ORR, and with argon for the HER. For the anodic reaction with a reaction area of 1 cm², pure C_2H_4 from a cylinder was used as gas feed unless otherwise stated. Catholyte and anolyte (both 2 M KCl) of constant volumes of 25 ml were circulated through the electrolyser with

a constant flow rate of 10 ml min⁻¹ using a peristaltic pump equipped with silicon tubing. Upon completion of electrolysis for 1 h, we collected the samples from the anolyte container and stored these in the sealed vials for 2 d in a refrigerator before further test. Calibration was carried out using diluted solutions of the potential electrolysis products: EO and HOC_2H_4Cl. Liquid products were analysed by high-performance liquid chromatography with a Thermo Scientific Dionex UltiMate 3000 and by NMR spectrometry (Agilent DD2 600 MHz) using dimethylsulfoxide as the internal standard. The CO_2RR performance assessment of the electrodes was made using a custom-made electrochemical test station: the station consisted of a potentiostat and a booster (Metrohm Autolab, 10 A) for the control of applied potential and current, a mass flow controller (Sierra, SmartTrak 100) for the supply of CO_2, a CO_2RR membrane electrode assembly electrolyser (Dioxide Materials) for electrochemical reaction, a humidifier for CO_2 humidification, and a peristaltic pump with silicon tubing for anolyte circulation. Chamber 1 comprised anode and cathode flow-field plates made of titanium and stainless steel. The geometric flow-field areas of the anode and cathode sides were 5 cm². The anode flow channels were responsible for the uniform supply of 0.1 M $KHCO_3$ anolyte while the cathode flow channels were responsible for the uniform supply of humidified CO_2. Before the electrochemical assessment, the anode and cathode electrodes were placed on their respective flow-field plates, and each bolt of the electrolyser was tightened by applying an equal compression torque. For the sake of good electrical contact, the cathode electrode was attached to its flow-field plate by using a copper tape frame, which was subsequently covered via a Kapton tape frame. The electrically conductive anode electrode was mounted firmly on its flow-field plate. The anion exchange membrane was activated in 1 M KOH for at least 24 h and soaked in water for 5 min before cell assembly. Following electrolyser assembly, 0.1 M $KHCO_3$ was circulated through the anode flow channels at a constant flow rate of 10 ml min⁻¹ with the aid of a peristaltic pump. The humidified CO_2 was fed into the cathode flow channels at a constant flow rate of 50 sccm using a mass flow controller unless otherwise stated. The reaction was then initiated by applying a current density of interest (100, 200 and 300 mA cm⁻²). The corresponding full-cell voltage for each current density applied was recorded while concurrently collecting the gas products of the CO_2RR via a gas-tight syringe (Hamilton chromatography syringe) in a constant 1 ml volume from the cathode outlet. The gas samples collected were injected into a gas chromatography system (PerkinElmer Clarus 680) comprising three main components: a flame ionization detector, a thermal conductivity detector and packed columns. The gas chromatography spectra obtained were utilized to calculate the FEs of the gas products, including H_2, CO, CH_4 and C_2H_4. For each current density, the gas product collection was performed at least three times at suitable time intervals. The FE was calculated from the equation: $FE (\%) = N \times F \times n/Q$ where N is the number of electrons transferred, F is the Faraday constant, n is the number of moles of product and Q is the total charge passed in electrochemical tests.

DFT calculations. Ab initio DFT calculations were performed by applying the projector augmented-wave method[22] as implemented in the Vienna Ab initio Simulation Package[23,24]. A plane-wave cutoff of 450 eV with a $2 \times 2 \times 1$ Monkhorst–Pack k-point grid[25] was applied for both IrO_2 and BaO_x/IrO_2. BaO_x/IrO_2 was modelled by depositing barium oxide clusters (Ba_3O_4) on a 12-atomic-layer (4×3) supercell of $IrO_2(200)$ surface with oxygen termination. We considered fully hydroxylated barium oxide clusters ($Ba_3O_4H_4$) because the saturation of oxygen atoms in metal oxide clusters is favoured in an electrochemical environment[26]. The atomic coordinates of the optimized models are provided in Supplementary Data 1. The zero damping DFT-D3 method of Grimme et al.[27] was used to ensure a good description of van der Waals interactions. A standard dipole correction was also included to decouple the electrostatic interaction between the periodic images[28]. During relaxation, atoms in the bottom-most six atomic layers of IrO_2 were fixed at their bulk positions, whereas other atoms were allowed to relax. All relaxations were considered to reach convergence until the Hellman–Feynman force on each ion was <0.01 eV Å⁻¹.

Data availability
The data supporting the findings of this study are available within the paper, the Supplementary Information and the source data files. Source data are provided with this paper.

References
1. De Luna, P. et al. What would it take for renewably powered electrosynthesis to displace petrochemical processes? *Science* **364**, eaav3506 (2019).
2. Zheng, J. & Suh, S. Strategies to reduce the global carbon footprint of plastics. *Nat. Clim. Chang.* **9**, 374–378 (2019).
3. *Direct CO_2 Emissions from Primary Chemical Production in the Sustainable Development Scenario, 2015–2030* (International Energy Agency, 2020); https://www.iea.org/data-and-statistics/charts/direct-co2-emissions-from-primary-chemical-production-in-the-sustainable-development-scenario-2015-2030
4. Boulamanti, A. & Moya Rivera, J. *Energy Efficiency and GHG Emissions: Prospective Scenarios for the Chemical and Petrochemical Industry* EUR 28471 EN, JRC105767 (Publications Office of the European Union, 2017).
5. Li, F. et al. Molecular tuning of CO_2-to-ethylene conversion. *Nature* **577**, 509–513 (2020).
6. Leow, W. R. et al. Chloride-mediated selective electrosynthesis of ethylene and propylene oxides at high current density. *Science* **368**, 1228–1233 (2020).
7. Barton, J. L. Electrification of the chemical industry. *Science* **368**, 1181–1182 (2020).
8. Chung, M., Jin, K., Zeng, J. S. & Manthiram, K. Mechanism of chlorine-mediated electrochemical ethylene oxidation in saline water. *ACS Catal.* **10**, 14015–14023 (2020).
9. Lum, Y. et al. Tuning OH binding energy enables selective electrochemical oxidation of ethylene to ethylene glycol. *Nat. Catal.* **3**, 14–22 (2020).
10. Zhuang, T.-T. et al. Dopant-tuned stabilization of intermediates promotes electrosynthesis of valuable C3 products. *Nat. Commun.* **10**, 4807 (2019).
11. Tachikawa, T., Beniya, A., Shigetoh, K. & Higashi, S. Relationship between OER activity and annealing temperature of sputter-deposited flat IrO_2 thin films. *Catal. Lett.* **150**, 1976–1984 (2020).
12. Touni, A., Papaderakis, A., Karfaridis, D., Vourlias, G. & Sotiropoulos, S. Oxygen evolution reaction at $IrO_2/Ir(Ni)$ film electrodes prepared by galvanic replacement and anodization: effect of precursor Ni film thickness. *Molecules* **24**, 2095 (2019).
13. Carrillo, A. J., Sastre, D., Serrano, D. P., Pizarro, P. & Coronado, J. M. Revisiting the BaO_2/BaO redox cycle for solar thermochemical energy storage. *Phys. Chem. Chem. Phys.* **18**, 8039–8048 (2016).
14. Nikolaeva, E. V., Zakiryanova, I. D., Korzun, I. V., Bovet, A. L. & Antonov, B. D. Interaction between barium oxide and barium containing chloride melt. *Z. Naturforsch.* **70**, 325–331 (2015).
15. Jouny, M., Luc, W. & Jiao, F. General techno-economic analysis of CO_2 electrolysis systems. *Ind. Eng. Chem. Res.* **57**, 2165–2177 (2018).
16. Israel, G. C., Martin, J. K. & Soper, F. G. The kinetics of chlorohydrin formation. Part I. The reaction between hypochlorous acid and allyl alcohol in aqueous solution. *J. Chem. Soc.* 1282–1285 (1950).
17. Pérez-Gallent, E. et al. Electroreduction of CO_2 to CO paired with 1,2-propanediol oxidation to lactic acid. Toward an economically feasible system. *Ind. Eng. Chem. Res.* **58**, 6195–6202 (2019).
18. Li, T., Cao, Y., He, J. & Berlinguette, C. P. Electrolytic CO_2 reduction in tandem with oxidative organic chemistry. *ACS Cent. Sci.* **3**, 778–783 (2017).
19. Llorente, M. J., Nguyen, B. H., Kubiak, C. P. & Moeller, K. D. Paired electrolysis in the simultaneous production of synthetic intermediates and substrates. *J. Am. Chem. Soc.* **138**, 15110–15113 (2016).
20. Wang, Y. et al. Simultaneous electrosynthesis of syngas and an aldehyde from CO_2 and an alcohol by molecular electrocatalysis. *ACS Appl. Energy Mater.* **2**, 97–101 (2019).
21. Bajada, M. A. et al. A precious-metal-free hybrid electrolyzer for alcohol oxidation coupled to CO_2-to-syngas conversion. *Angew. Chem. Int. Ed.* **59**, 15633–15641 (2020).
22. Kresse, G. & Joubert, D. From ultrasoft pseudopotentials to the projector augmented-wave method. *Phys. Rev. B* **59**, 1758–1775 (1999).
23. Kohn, W. & Sham, L. J. Self-consistent equations including exchange and correlation effects. *Phys. Rev.* **140**, A1133–A1138 (1965).
24. Kresse, G. & Furthmüller, J. Efficient iterative schemes for ab initio total-energy calculations using a plane-wave basis set. *Phys. Rev. B* **54**, 11169–11186 (1996).
25. Monkhorst, H. J. & Pack, J. D. Special points for Brillouin-zone integrations. *Phys. Rev. B* **13**, 5188–5192 (1976).
26. Zhou, B. et al. Highly efficient binary copper–iron catalyst for photoelectrochemical carbon dioxide reduction toward methane. *Proc. Natl Acad. Sci. USA* **117**, 1330–1338 (2020).
27. Grimme, S., Antony, J., Ehrlich, S. & Krieg, H. A consistent and accurate ab initio parametrization of density functional dispersion correction (DFT-D) for the 94 elements H–Pu. *J. Chem. Phys.* **132**, 154104 (2010).
28. Neugebauer, J. & Scheffler, M. Adsorbate–substrate and adsorbate–adsorbate interactions of Na and K adlayers on Al(111). *Phys. Rev. B* **46**, 16067–16080 (1992).

Author contributions
C.L. and E.H.S. supervised the project. Y. Li, A.O. and W.R.L. conceived the idea and designed and carried out the experiments. Y. Li and W.R.L. collected STEM and TEM

images and carried out energy-dispersive X-ray spectroscopy mapping. P.O. carried out theoretical calculations. Y.X. fabricated the customized flow cell. Y. Liu and K.B. performed X-ray diffraction and XPS measurements. A.O. carried out analysis of CO_2RR products. Y. Li and W.R.L. analysed ethylene chlorohydrin and EO products. J.E.H., Y.W., C.R., H.J. and D.S. contributed to data analysis and manuscript editing. Y. Li, C.L. and E.H.S. co-wrote the paper. All authors discussed the results and assisted during manuscript preparation.

Competing interests

Y. Li, A.O., W.R.L, P.O. and E.H.S. have filed provisional patent application number 63/265.897 regarding the electrosynthesis of oxiranes. The other authors declare no competing interests.

Additional information

Supplementary information The online version contains supplementary material available at https://doi.org/10.1038/s41929-022-00749-8.

Correspondence and requests for materials should be addressed to Chunzhong Li or Edward H. Sargent.

Peer review information *Nature Catalysis* thanks the anonymous reviewers for their contribution to the peer review of this work.

Reprints and permissions information is available at www.nature.com/reprints.

Publisher's note Springer Nature remains neutral with regard to jurisdictional claims in published maps and institutional affiliations.